Effect of grain boundaries on mechanical transverse wave propagations in graphene

Jun Xia, YinBo Zhu,[a)] FengChao Wang, and HengAn Wu[a)]
CAS Key Laboratory of Mechanical Behavior and Design of Materials, Department of Modern Mechanics,
CAS Center for Excellence in Nanoscience, University of Science and Technology of China, Hefei,
Anhui 230027, China

The effects of grain boundary (GB) on the mechanical transverse wave propagation in graphene are studied via molecular dynamics simulations and frequency spectrum analysis. We reveal that GB can attenuate transverse waves at terahertz frequencies in graphene, which might be significant for manipulating terahertz noises via nanostructured modifications in graphene-based nanodevices. Two fundamental mechanisms, scattering and resonance, are found in the attenuation of terahertz waves. The scattering impairs waves slightly with a wide range of effective frequencies, whereas the resonance, occurring in the vicinity of GB, significantly reduces the amplitude responses near resonance frequencies, which displays a special frequency-selective filter-like behavior. Moreover, the strong correlation between amplitude loss and buckling height further demonstrates the effects of GB on terahertz mechanical waves in graphene with different chiralities and misorientation angles. *Published by AIP Publishing.* [http://dx.doi.org/10.1063/1.4984763]

I. INTRODUCTION

Over the past decades, propagation of acoustic waves in periodic structures[1–4] has received much attention because of renewed physical properties, applications in noise and vibration isolation,[5,6] frequency filters in wireless communication, etc. Graphene, due to its two-dimensional nature and extraordinary electronic, thermal, and mechanical properties, has been widely applied in sensors,[7] resonators,[8] superconductors,[9] and nanoelectromechanical devices,[10] especially in some sonic and thermal devices.[1] It is an excellent medium for surface acoustic wave propagations which contribute to two-dimensional electron systems, communication systems, and sensing.[11]

Generally, precise nanosensors and devices are susceptible to the effects of acoustic noises,[6] in particular, high frequency terahertz noises. Therefore, the ability to control and attenuate the acoustic waves would allow the creation of nanoscale devices with an improved performance or a new functionality. Macroscale and microstructured materials are known enough to control sound, ultrasound, and hypersound waves, whereas to manipulate the mechanical waves of much higher frequencies (>0.1 THz), nanostructured modifications are necessarily required.[1,12,13] One approach to modify the graphene nanostructure is to introduce structural defects,[14] such as GBs, known to exist ubiquitously in graphene. The experimental studies have shown that dislocations can be introduced into graphene using a focused electron beam,[15] guaranteeing the possibility of modification at nanoscale.

GB, like other structural defects, is found to affect the electronic transport,[16–19] thermal,[20–24] and mechanical properties[25–27] of graphene and is thus widely used in tuning these properties. The existence of GBs can induce out-of-plane buckling in graphene.[16,20,28,29] The tilt GB in graphene is known to consist of a series of pentagon-heptagon pairs, in which the defect density is determined by the misorientation angle (θ). Over the past few years, the effects of GB on the phonons transport, which are especially important for designing materials to manipulate phonon particles, have been investigated.[30–34] However, these studies place emphasis on the thermal transport properties and give no detailed insight into the case of terahertz range frequencies. Out of these studies, Liu *et al.*,[12] who considered the chirality difference, reported that the graphene can manipulate terahertz mechanical waves. The understanding of the performance of graphene sheet under high frequency vibrations was reached in the recent studies,[35] whereas the effects of GB on attenuating terahertz mechanical waves in graphene and associated vibration performances remain unclear. Our work on attenuating terahertz waves via GBs may result in an accessible strategy for controlling high frequency waves by nanostructured modifications.

In this paper, we utilize molecular dynamics (MD) simulation and frequency spectrum analysis to investigate the effect of GB on the transverse wave propagation in graphene. Our results reveal the manipulation of terahertz mechanical waves in graphene through two underlying attenuation mechanisms, i.e., scattering and resonance, which are found remarkably effective in terahertz frequency range. The scattering-induced attenuation can impair waves slightly and be well described by Rayleigh scattering in a certain frequency range, whereas the resonance-induced attenuation can significantly reduce the amplitude response. Moreover, to understand the effect of buckling heights, we also calculate amplitude responses at different graphene chiralities and misorientation angles for comparison.

a)Authors to whom correspondence should be addressed: zhuyinbo@mail.ustc.edu.cn and wuha@ustc.edu.cn

II. METHODOLOGY

As illustrated in Fig. 1, we established armchair- and zigzag-oriented GB models with different misorientation angles. These GB structures were obtained by "sewing" method,[25] in which two misoriented graphene sheets were stitched together. Then, energy minimization was performed by MD simulations, using the program package named LAMMPS.[36] The optimized Tersoff potentials proposed by Lindsay and Broido,[37] shown to improve the accuracy of lattice dynamics and acoustic vibration calculations, were used to describe the carbon-carbon interactions. To enable a full relaxation, the size of the simulation box in the x and y directions are allowed to vary independently of each other. However, the energy minimization algorithm (molecular mechanics) in LAMMPS cannot produce the buckled GB, as reported in Refs. 31 and 32. Therefore, we introduce a small thermal perturbation via molecular dynamics: the optimized structures were finally equilibrated at 0.01 K for 10 ns in the *NPT* ensemble. Equilibrating at a higher or lower temperature does not change the GB structure or buckling characteristics. Periodic boundary conditions (PBCs) were imposed on all the three directions of the simulation box during energy minimization and thermal equilibration; thus, one supercell should contain two GBs (one GB is in the middle of the supercell, while the other one is in the boundary). The schematic plot of GB supercells (considering the long size of x direction, just the center part of the unit cell is shown) is illustrated in Figs. 1(c)–1(f). As the GBs mentioned in this paper is all periodic and increasing the y direction size to more than one grain boundary period has no effect on the buckling characteristics,[31] the supercells are chosen to own 1 or 2 GB periods in the y direction to reduce the computation cost. The system length in the x direction, which is found to greatly influence the buckling degree, should be appropriate to be $\sim$300 nm.[31] The optimization results, shown in Figs. 1(e) and 1(f), all exhibit substantial out-of-plane buckling heights up to 0.7 nm, which are in good agreement with the results in Ref. 31.

To reveal the mechanism of terahertz transverse waves via GBs, we applied a sinusoidal excitation to carbon atoms on one side 75 nm away from GB, while we collected amplitude responses on the other side 25 nm away from GB. To avoid the PBCs-induced cross-boundary wave interfering with the original wave, which causes the distortion of the signal, we fine-tune the simulation method when studying the propagation of transverse waves. In detail, fixed boundary conditions were imposed in the x and z directions, and the PBC was set in the y direction. The coordinates of atoms less than 10 nm away from the two edges were frozen. We only consider the wave propagation before the wave reflects on supercell edges. The mechanical excitation was applied to carbon atoms in a rectangular region, which is infinite in the y direction (due to PBC) and is 1 nm in the x direction. The sinusoidal waveform was in the longitudinal displacement direction (the z direction) of selected carbon atoms, and the wave propagation direction is then perpendicular to the displacement direction, i.e., the transverse wave mode. The *NVE* ensemble (constant number of atoms, volume, and energy; microcanonical ensemble) was used during the propagation of transverse waves. The frequency range explored in this work is 0.02–1.5 THz. The amplitude was set 0.01 nm to avoid the nonlinear effects.[31,38,39] In this study, since we only consider conditions before the wave reflects on supercell edges, long x direction size is very necessary for terahertz waves to propagate for a certain time, helping to collect data for frequency spectrum analysis. The frequency spectrum analysis (amplitude–frequency response) is performed by fast Fourier transform (FFT), in which the time-dependent atom displacements of the discrete signal in the z direction was acquired and then processed. The amplitude loss is defined as

$$dB = 10\log_{10}(A_1^2/A_0^2) = 20\log_{10}(A_1/A_0), \qquad (1)$$

where A_1 denotes the simulated amplitude response and A_0 denotes the reference amplitude.
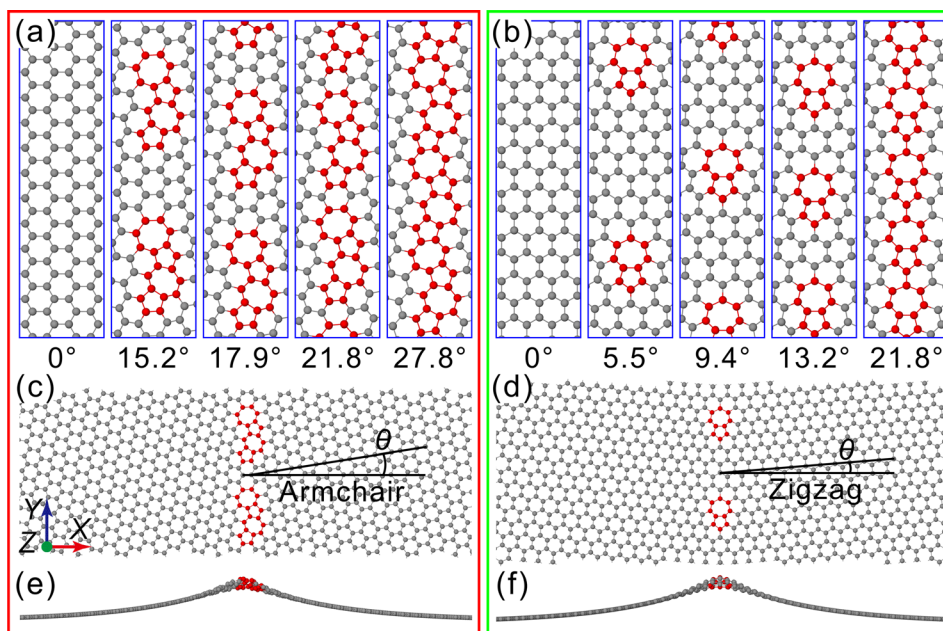

FIG. 1. Examined graphene GBs constructed by "sewing" method. (a) and (b) Armchair- and zigzag-oriented GB structures with different misorientation angles, respectively. (c)–(f) Schematic plot of the GB supercells (considering the long size of x direction, just the center part of the unit cell is shown). Actually, one supercell should contain two GBs (one GB is in the middle of the supercell, while the other one is in the boundary). The top and bottom figures are viewed from z and y directions, respectively.
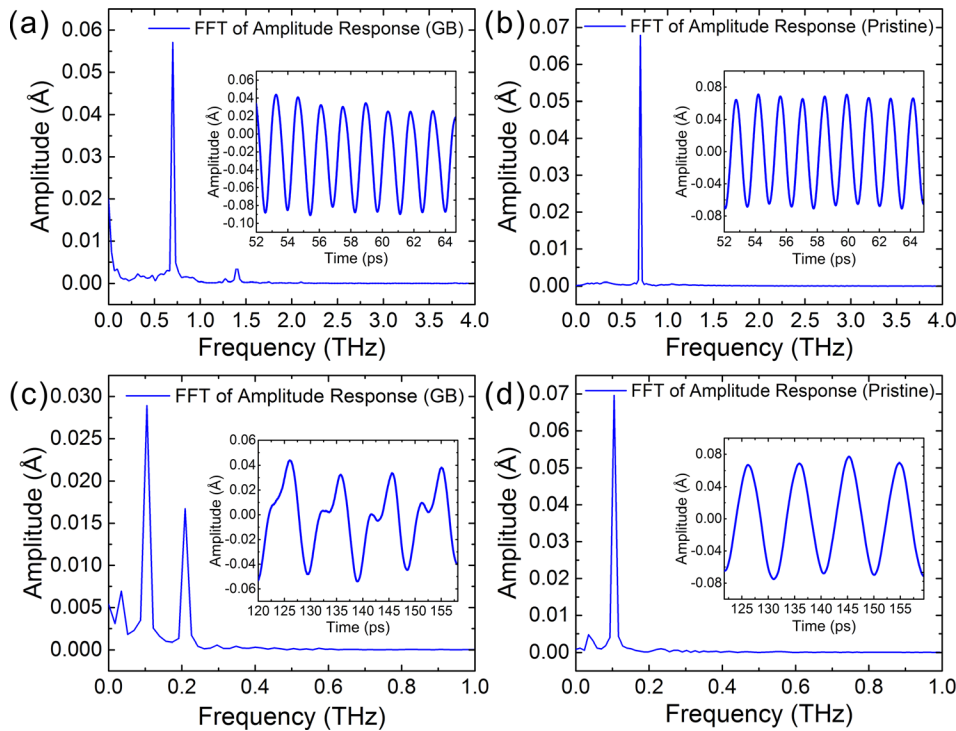
FIG. 2. Two attenuation mechanisms found in our simulations. (a) and (b) FFT results of scattering ($f = 0.7$ THz) in graphene with and without GB, respectively. (c) and (d) FFT results of resonance ($f = 0.105$ THz) in graphene with and without GB, respectively. The insets in (a)–(d) illustrate the amplitude responses after transverse waves went through GBs.

III. RESULTS AND DISCUSSION

Here, due to the similar characteristics presented in different GBs, we take the result of armchair-oriented GB with $\theta = 15.2°$ as an example to reveal the essential effect of GB on terahertz wave propagations in graphene. Amplitude responses and their FFT results are plotted in Fig. 2. Interestingly, two different attenuation mechanisms are found in our simulations. One mechanism is the scattering-induced attenuation. Figures 2(a) and 2(b) compare the results in graphene with and without GB when the signal frequency (f) is 0.7 THz. In this mechanism, waves are attenuated after going through GBs with few clutters, although the attenuation effect is extremely weak. The other one is the resonance-induced attenuation. As shown in Figs. 2(c) and 2(d) with $f = 0.105$ THz, waves are dramatically weakened. As a comparable second harmonic peak with the original signal appears in the frequency spectrogram, a resonance should have happened during the wave propagation and introduced higher harmonic wave components into the amplitude response [the inset in Fig. 2(c)].

As terahertz waves can be attenuated through the two different attenuation mechanisms via GBs at nanoscale, the size of GB is surely considerable to the wavelength of transverse waves in terahertz frequency range. Thus, the simulated amplitude losses induced by GBs should show a component proportional to the frequency (hysteresis loss) and another proportional to the fourth power of frequency (Rayleigh scattering).[40,41] To better clarify the scattering effects of GBs, we summarize the FFT results in the frequency range from 0.02 to 1.5 THz and show the amplitude loss curves in Fig. 3. The inset compares this range with two wavebands, the hypersound and the heat. The frequency range studied in this letter is mainly at the heat waveband (terahertz). As we note that the existence of resonance will greatly affect the amplitude

responses near resonant points, we temporarily exclude these results and shall discuss in detail later.

The black line with solid circle symbols in Fig. 3 denotes the transverse wave propagation in the pristine graphene sheet. It is previously reported that, without GBs, the graphene inherently possesses the ability to manipulate and attenuate terahertz waves.[12] Similarly, weak attenuation is found and confirmed in our simulations, and this effect strengthens gradually with the increase in the frequencies. In the case of the graphene with GBs, however, the wave amplitude loss manifests a tremendous variation with the increase in the frequencies. The results marked by red squares can be
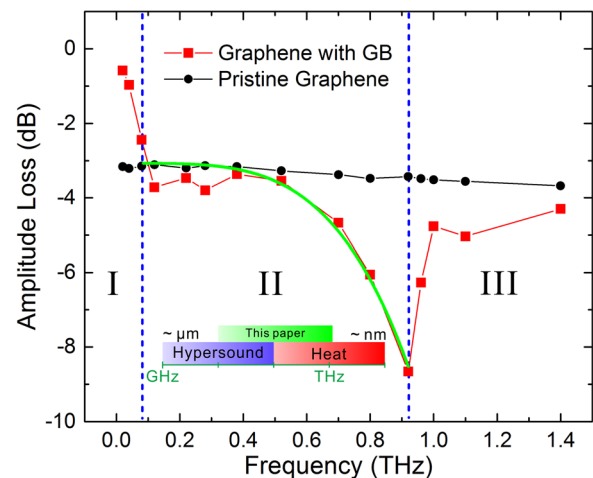

FIG. 3. Results of the amplitude loss in the frequency range from 0.02 to 1.5 THz, taking no account of the data points which are greatly affected by resonance. The results can be clearly divided into three stages. The inset compares the frequency range studied in this letter with two wavebands, the hypersound and the heat. The green curve is fitted based on Rayleigh scattering theory.

obviously divided into three stages: stage I ($f < 0.08$ THz) shows an "enhancement" of amplitude with decreased frequencies. It is strange that the amplitude loss in graphene with GBs is much smaller than that in the pristine graphene; stage II (0.08 THz $< f < 0.92$ THz) displays a relatively low attenuation which can be well described by the classical Rayleigh scattering theory; in stage III ($f > 0.92$ THz), the theory fails, with amplitude losses tending to be lifted and disordered. As the wavelength of the transverse wave in stages I and II is much smaller than the size of GB, according to Rayleigh's scattering theory, the simulated amplitude losses should show a component proportional to the frequency and another proportional to the fourth power of frequency. Therefore, we can fit the curve in stage II by the polynomial[40]

$$\alpha = af + bf^4 + c, \quad (2)$$

where α is the attenuation coefficient (that is, the amplitude loss) and c is the attenuation ability of the pristine graphene. As the amplitude loss curve of the pristine graphene shows a little variation in stage II, we set c as a constant ($c \approx 3.07$ dB). When the frequency is low (0.08–0.4 THz), the fitting curve is found far away from the data points, while it fits well at high frequencies (0.4–0.92 THz). This irregularity in the frequency range from 0.08 to 0.4 THz is evident due to the influence of other-mechanism-induced attenuation. Moreover, there is also something unclear in stage III.

The red curve in Fig. 3 indicates an apparent band-stop-filter-like function in spite of relatively low attenuation ability. Subsequently, to gain more insight into the three stages and the band-stop-filter-like phenomenon in Fig. 3, we take the effect of resonance-induced attenuation into account. Figure 4(a) shows the amplitude loss in the frequency range

from 0.02 to 0.4 THz, considering those results affected by resonance. As shown in Fig. 4(b), in stage I, the amplitude responses before and after the wave went through GB show a little difference. Actually, the waves in stage I belong to the hypersound waveband, whose wavelength is considerably larger than the size of GB. Thus, it is certain that the waves are hardly affected by GBs. But, a natural question arises: what mechanism contributes to the "enhancement"? We think that various factors contribute to this abnormity. On the one hand, the waves are less attenuated compared with stages II and III, with less energy dissipated to low-frequency modes. On the other hand, we speculate that the existence of GB changes the natural frequency of graphene sheet, just like that the GB splits a graphene sheet into two parts. According to Ref. 35, the natural frequency of a graphene sheet with 150 nm in length is smaller than 0.05 THz. Therefore, the frequencies in stage I are close to this natural value, which causes the "enhancement" phenomenon. One evidence is that a low second harmonic peak is found in the FFT results before the waves went through GBs, although it is attenuated by GBs after the waves went through GBs [Fig. 4(b)]. This harmonic component should result from the resonance of graphene sheet.

When it comes to stage II, there exist two regions: one region (0.4–0.92 THz) can be well described by Rayleigh scattering theory and the other one (0.08–0.4 THz) is displayed in Fig. 4(a). Resonance actually occurs throughout the terahertz frequency range, but in this low frequency range, dense resonance peaks exist and dramatically influence the amplitude response. Compared with the results in Fig. 3, the attenuation caused by resonance is much more critical, up to 30 dB. To validate the fact that the resonances are induced by GBs, we check amplitude responses at several checkpoints. The amplitude response is merely found locally
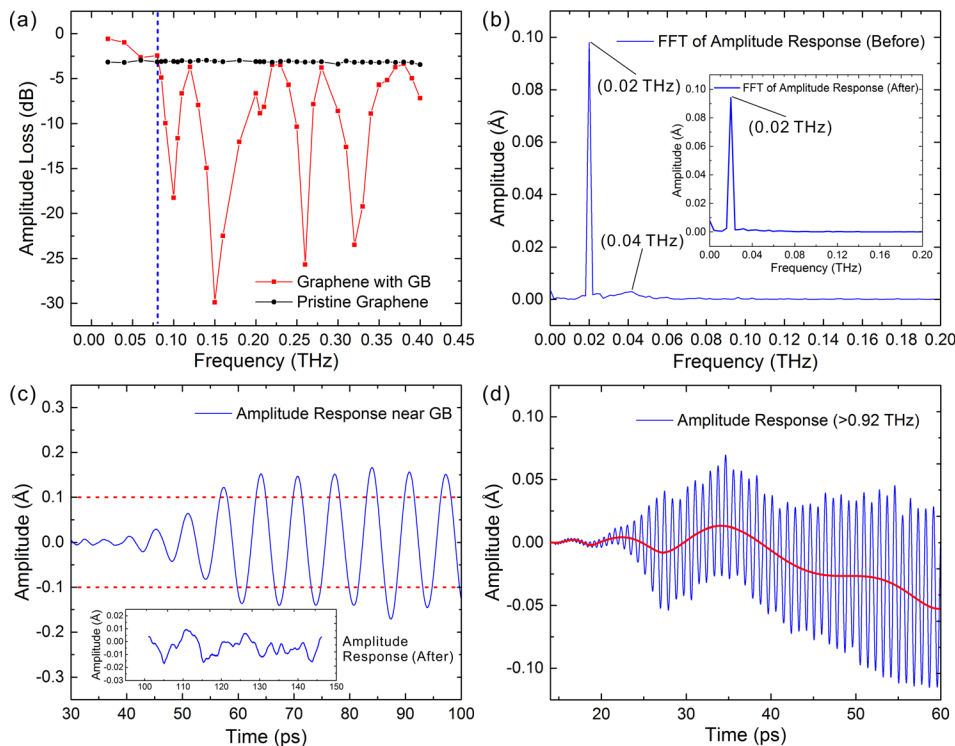

FIG. 4. (a) Amplitude loss in the frequency range from 0.02 to 0.4 THz, taking into account the data points affected by resonance. (b) Comparison of the FFT results of amplitude responses before and after the waves went through GBs in stage I. (c) Local resonance occurring in the vicinity of GBs in stage II. The inset is the amplitude response collected after waves went through GBs. (d) Fluctuations of amplitude responses in stage III.

strengthened in the vicinity of GB [Fig. 4(c)]. After that, the transverse wave seems to be trapped and little of it can go through GB. In this mechanism, wave resonates with GB in the GB region, causing the destabilization of GB, during which a quantity of mechanical energy is converted into thermal energy. Thus, as illustrated in the inset in Fig. 4(c), the sinusoidal waves become a combination of original waves (attenuated), higher harmonic components, and destabilization-induced noise waves after going through GB. In this way, the input signals are extremely attenuated at resonance frequencies by at least one order of magnitude. As mentioned above, GB can be utilized in graphene-based band-stop-filter-like nanodevices despite the low attenuation efficiency as a result of scattering-based attenuation. Here, due to this special frequency-selective filtering behavior induced by resonance mechanism, we can dramatically increase its efficiency in mechanical wave attenuation [in this paper, band-stop ranging from 0.7 to 1.0 THz, with the attenuation high up to 30–40 dB (resonance caused)] and extend it to some other applications of particular purposes.

In stage III, the wavelength becomes comparable to the GB size; thus, the scattering loss should increase more closely with the square of the frequency.[40] Actually, the red median line in Fig. 4(d) reveals a considerable fluctuation of graphene sheet when the wave frequency is over 0.92 THz, indicating the intensification of GB destabilization. The destabilization gradually propagates to the whole graphene sheet, which greatly enhances the amplitude response. Simultaneously, stage III is also affected by the resonance of GB. That is, several factors jointly contribute to the complicated amplitude responses in stage III. In the frequency range ($f < 2.0$ THz) studied in this letter, the qualitative regularity of the amplitude response almost presents no difference, in spite of different graphene orientation or misorientation angles, whereas when the frequency increases ($f > 3.0$ THz), the amplitude response will show more distinct and novel characteristics, varying with different chiralities.[12]

Although transverse waves show similar characteristics when they go through different GBs, there still exist some distinctions. Actually, different GBs are classified by chirality and orientation, which also affect the buckling height of GB. To further understand the inherent relationship, we summarize the FFT results of different GBs at a same signal frequency ($f = 0.1$ THz). As the effect of grain size on the scattering behaviors has been studied previously,[41,42] here we only discuss the effect on the resonance mechanism. Figures 5(a) and 5(b) show the comparisons of amplitude loss and buckling height at the resonant point. It is found that amplitude loss is positively related to the buckling height. In addition, comparing the amplitude losses in armchair- and zigzag-oriented graphene sheets, we find that GBs in zigzag-oriented graphene sheets have much stronger attenuation ability than those in armchair-oriented graphene, although their buckling heights are similar. For instance, the armchair-oriented graphene with GB misorientation angle $\theta = 27.8°$ (armchair-27.8) and zigzag-oriented graphene with $\theta = 21.8°$ (zigzag-21.8) are nearly flat in the GB region. Therefore, it seems that these two GBs should behave like the similarly flat pristine graphene sheet. In general, a pristine graphene sheet has extremely weak attenuation effect on the transverse wave at low frequencies. However, the results in Fig. 5(b) show that zigzag-21.8 attenuates waves more significantly than similarly flat armchair-27.8 pristine graphene. We find that it should be attributed to the chirality-difference-induced symmetry difference. The armchair-27.8 shown in Fig. 5(c) possesses left-right asymmetry, while the zigzag-21.8 in Fig. 5(d) is bilaterally symmetric. This bilateral symmetry induces the folding of bilateral misoriented graphene sheets, as shown in the inset in Fig. 5(d). Then, the folding further introduces a small local buckling in the GB region, which slightly enhances the attenuation ability of GB. The dependence of attenuation effects on graphene chiralities and GB buckling heights provides a method to adjust the performance of graphene-based nanodevices.
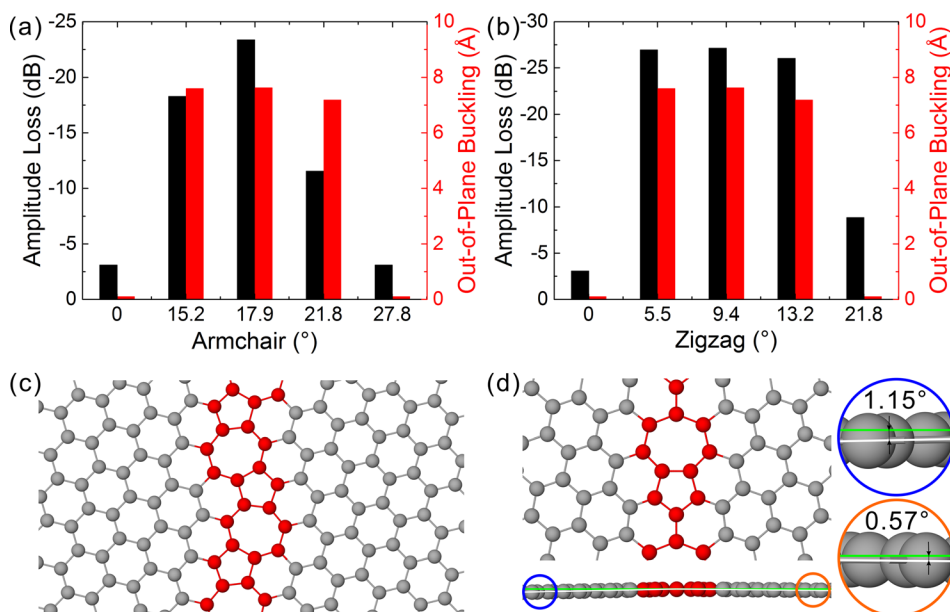

FIG. 5. (a) and (b) Comparison of the amplitude loss and GB buckling height in graphene sheets with different chiralities and misorientation angles. (c) and (d) Symmetry comparison of the two GBs (armchair-27.8 and zigzag-21.8). The inset in (d) displays the folding of bilateral misoriented graphene sheets.

IV. CONCLUSION

In summary, using MD simulations and frequency spectrum analysis, we investigate that the effect of GB on the mechanical transverse wave propagation in graphene. GB is found to attenuate waves at terahertz frequencies with two fundamental mechanisms, i.e., scattering and resonance. The scattering-induced attenuation can impair waves with a wide range of effective frequencies and be well described by Rayleigh scattering theory in a certain frequency range. Whereas, the resonance-induced attenuation shows a special frequency-selective filter-like behavior, in which the amplitude response is significantly reduced near resonance frequencies, by the local resonance occurring in the vicinity of GB. When the signal frequency is larger than a critical limit, the resonance-induced destabilization of GB tends to propagate to the whole graphene, resulting in the distortion in amplitude response. Moreover, the comparison of terahertz wave attenuation in graphene with different chiralities and misorientation angles indicates the positive correlation between amplitude loss and buckling height, which further demonstrates the effects of GB on terahertz mechanical waves in graphene. It is also found that the zigzag-oriented GBs generally exhibit much stronger attenuation ability than armchair-oriented GBs. These investigations of transverse wave propagation through GBs should provide a strategy to manipulate the terahertz mechanical noises by designing GBs and their buckling heights in graphene-based nanodevices.

[1]M. Maldovan, Nature **503**, 209 (2013).
[2]X. Li, F. Wu, H. Hu, S. Zhong, and Y. Liu, J. Phys. D: Appl. Phys. **36**, L15 (2003).
[3]Y. Tanaka and S. Tamura, Phys. Rev. B **58**, 7958 (1998).
[4]M. Kafesaki and E. N. Economou, Phys. Rev. B **60**, 11993 (1999).
[5]S. S. Rao and F. F. Yap, *Mechanical Vibrations* (Prentice Hall, Upper Saddle River, 2011).
[6]W. N. Yunker, C. B. Stevens, G. T. Flowers, and R. N. Dean, J. Appl. Phys. **113**, 024906 (2013).
[7]F. Schedin, A. K. Geim, S. V. Morozov, E. W. Hill, P. Blake, M. I. Katsnelson, and K. S. Novoselov, Nat. Mater. **6**, 652 (2007).
[8]J. S. Bunch, A. M. van der Zande, S. S. Verbridge, I. W. Frank, D. M. Tanenbaum, J. M. Parpia, H. G. Craighead, and P. L. McEuen, Science **315**, 490 (2007).
[9]J. Trbovic, N. Minder, F. Freitag, and C. Schönenberger, Nanotechnology **21**, 274005 (2010).
[10]J. S. Bunch, S. S. Verbridge, J. S. Alden, A. M. van der Zande, J. M. Parpia, H. G. Craighead, and P. L. McEuen, Nano Lett. **8**, 2458 (2008).
[11]D. Roshchupkin, L. Ortega, I. Zizak, O. Plotitcyna, V. Matveev, O. Kononenko, E. Emelin, A. Erko, K. Tynyshtykbayev, D. Irzhak, and Z. Insepov, J. Appl. Phys. **118**, 104901 (2015).
[12]X. Liu, F. Wang, and H. Wu, Appl. Phys. Lett. **103**, 071904 (2013).
[13]A. Smolyanitsky and V. K. Tewary, Nanotechnology **24**, 055701 (2013).
[14]J. Xia, X. Liu, W. Zhou, F. Wang, and H. Wu, Nanotechnology **27**, 274004 (2016).
[15]J. H. Warner, Y. Fan, A. W. Robertson, K. He, E. Yoon, and G. D. Lee, Nano Lett. **13**, 4937 (2013).
[16]T. H. Liu, G. Gajewski, C. W. Pao, and C. C. Chang, Carbon **49**, 2306 (2011).
[17]P. Vancsó, G. I. Márk, P. Lambin, A. Mayer, C. Hwang, and L. P. Biró, Appl. Surf. Sci. **291**, 58 (2014).
[18]J. Lahiri, Y. Lin, P. Bozkurt, I. I. Oleynik, and M. Batzill, Nat. Nanotechnol. **5**, 326 (2010).
[19]Z. Zhu, Z. G. Fthenakis, and D. Tománek, 2D Mater. **2**, 035001 (2015).
[20]O. V. Yazyev and S. G. Louie, Phys. Rev. B **81**, 195420 (2010).
[21]A. Y. Serov, Z. Y. Ong, and E. Pop, Appl. Phys. Lett. **102**, 033104 (2013).
[22]Z. G. Fthenakis and D. Tománek, Phys. Rev. B **86**, 125418 (2012).
[23]Z. G. Fthenakis, Z. Zhu, and D. Tománek, Phys. Rev. B **89**, 125421 (2014).
[24]Y. Lu and J. Guo, Appl. Phys. Lett. **101**, 043112 (2012).
[25]N. Xu, J. G. Guo, and Z. Cui, Physica E **84**, 168 (2016).
[26]R. Grantab, V. B. Shenoy, and R. S. Ruoff, Science **330**, 946 (2010).
[27]X. Liu, F. Wang, and H. Wu, Phys. Chem. Chem. Phys. **17**, 31911 (2015).
[28]A. Capasso, E. Placidi, H. F. Zhan, E. Perfetto, J. M. Bell, Y. T. Gu, and N. Motta, Carbon **68**, 330 (2014).
[29]X. Liu, F. Wang, and H. Wu, Nanotechnology **26**, 065701 (2015).
[30]P. K. Schelling, S. R. Phillpot, and P. Keblinski, Appl. Phys. Lett. **80**, 2484 (2002).
[31]E. E. Helgee and A. Isacsson, Phys. Rev. B **90**, 045416 (2014).
[32]E. E. Helgee and A. Isacsson, Phys. Rev. B **91**, 205432 (2015).
[33]C. Kimmer, S. Aubry, A. Skye, and P. K. Schelling, Phys. Rev. B **75**, 144105 (2007).
[34]A. Bagri, S. P. Kim, R. S. Ruoff, and V. B. Shenoy, Nano Lett. **11**, 3917 (2011).
[35]R. Chowdhury, S. Adhikari, F. Scarpa, and M. I. Friswell, J. Phys. D: Appl. Phys. **44**, 205401 (2011).
[36]S. Plimpton, J. Comput. Phys. **117**, 1 (1995).
[37]L. Lindsay and D. A. Broido, Phys. Rev. B **81**, 205441 (2010).
[38]S. Y. Kim and H. S. Park, J. Appl. Phys. **110**, 054324 (2011).
[39]J. Lee, V. Varshney, J. S. Brown, A. K. Roy, and B. L. Farmer, Appl. Phys. Lett. **100**, 183111 (2012).
[40]W. P. Mason and H. J. McSkimin, J. Acoust. Soc. Am. **19**, 464 (1947).
[41]H. Ogi, M. Hirao, and T. Honda, J. Acoust. Soc. Am. **98**, 458 (1995).
[42]A. G. Evans, B. R. Tittmann, L. Ahlberg, B. T. Khuri-Yakub, and G. S. Kino, J. Appl. Phys. **49**, 2669 (1978).